J. Electrochem. Sci. Eng. **12(4)** (2022) 777-786; http://dx.doi.org/10.5599/jese.1353

Open Access : : ISSN 1847-9286
https://pub.iapchem.org/ojs/index.php/JESE

Original scientific paper

Cubic like $CoMn_2O_4$ nanostructures as advanced high-performance pseudocapacitive electrode

Puratchimani Mani[1], Venkatachalam Vellaikasi[2,✉], Xavier Thankappan Suryabai[3], Abraham Rajasekar Simon[2] and Thamizharasan Kattaiyan[2]

[1]*Department of Physics, As-Salam College of Engineering and Technology, Thirumangalakudi, Aduthurai- 612 012. India*
[2]*Department of Physics, Sir Theagaraya College, Chennai -600 025, India*
[3]*Department of Physics, Centre for Advanced Material Research, Govt. College for Women, Thiruvananthapuram, Kerala- 695014, India*

Corresponding author: ✉venkatcnst12@gmail.com

Received: April 24, 2022; Accepted: June 21, 2022; Published: July 18, 2022

Abstract

In this work, a synthesis of cubic-like $CoMn_2O_4$ uniform nanostructures with KOH-NaOH involved in the hydrothermal method has been reported. The crystal structure phase purity, functional groups, and morphology of the $CoMn_2O_4$ have been investigated by X-ray diffraction (XRD), field emission scanning electron microscopy (FE-SEM), high-resolution transmission electron microscopy (HR-TEM) analyses. The electrochemical behaviour of $CoMn_2O_4$ electroactive material has been examined for supercapacitors. The electrode displays excellent capacitive behaviour with superior electrochemical properties. The cubic-like morphology structure with enough free space is beneficial for improving electrochemical performance. The $CoMn_2O_4$ electrode exhibits a faradaic capacitance with the highest specific capacitance value of 762.4 F g^{-1} at a scan rate of 5 mV s^{-1}. The coulombic efficiency of the $CoMn_2O_4$ electrode was found to be 91.2 % after 2000 charging-discharging cycles. The nanostructures of $CoMn_2O_4$ make a prominent contrib0-ution to the excellent electrochemical performance of the prepared electrode.

Keywords

Hydrothermal method; faradaic capacitance; long-term stability; energy storage

Introduction

In recent years, supercapacitors (SCs) have been focused on energy storage applications due to their distinctive advantages such as low cost, high-energy density, rapid charge-discharge rates, and environmental benignity when compared to batteries. The choice of electrode materials plays an important role in determining SC behaviour. These factors have triggered a significant research interest in the development and design of new and superior electrode materials for supercapacitors.

Among numerous available electrode materials, binary metal oxides with excellent electrochemical performance were found to be promising, effective, and scalable alternatives. In addition, binary metal oxides possess achievable oxidation states, high electrical conductivities, excellent electrochemical properties, and moreover, they are affordable and environmentally friendly when compared to single-component oxides.

In general, transition metal oxides with multiple oxidation states undergoing some redox reactions were already being used as pseudocapacitive or faradaic materials [1-3]. A huge interest has been put towards the synthesis and development of metal-oxide nanostructures with excellent electrochemical properties. Simple binary metal oxide electrode materials such as MnO_2 [4], Co_3O_4 [5] and NiO [6] have been widely studied as electrode materials for supercapacitor with excellent electrochemical behaviour. Meanwhile, ternary metal oxides with different metal cations like $CoFe_2O_4$, $FeMn_2O_4$, $MnCo_2O_4$ and $NiFe_2O_4$ have also attracted attention because of their promising applications in the energy storage field [7-11]. The coupling of two metal species might increase oxidation-state-rich redox reactions crucial for pseudocapacitors and different combinations of cations during the charging-discharging process could provide great opportunities to manipulate the physical and chemical properties of electrodes.

$CoMn_2O_4$ has already been considered a promising material for supercapacitors owing to its outstanding reversible capacity and widespread availability. The Co_2MnO_4 material is found to exhibit an excellent capacitive behavior because cobalt exhibits higher oxidation potential while manganese can transport more electrons [12]. For example, Jiang *et al*. [13] reported the growth of cobalt-manganese composite oxide nanostructures on Ni foam by hydrothermal method, displaying specific capacitance of even 840.2 F g^{-1} at a current density of 10 A g^{-1} and showing the excellent cycling performance. Ren and his co-workers [14] have reported the solvothermal synthesized uniform and decentralized flower-like $CoMn_2O_4$ of hierarchical nanostructures that exhibited a specific capacitance of 188 F g^{-1} in Na_2SO_4 solution.

Metal oxide nanostructures as supercapacitor electrodes are fascinating owing to their large surface area and reduced particle size, which generates more interfacial active sites. Various synthesis methods for the preparation of metal oxide nanostructures have been widely explored, including the co-precipitation technique, hydrothermal method, template-assisted synthesis, and electrochemical deposition. Among these methods, hydrothermal is a powerful method to synthesize nanostructures, where the size, crystal structure, and morphology of the product materials can easily be controlled.

Herein, we have developed a facile method to prepare $CoMn_2O_4$ nanostructured material by the hydrothermal method, involving potassium and/or sodium hydroxide solution treatment. The prepared material has been characterized by some surface techniques, while its pseudocapacitive and stability properties are determined by CV and galvanostatic charging-discharging experiments.

Experimental

Material synthesis

$CoMn_2O_4$ nanostructures were prepared using double-hydroxide treatment involved in the hydrothermal method. The material was synthesized as follows: initially, 9 g of mixed hydroxides solution was prepared by adding an equal molar ratio of potassium hydroxide (KOH) and Sodium hydroxide (NaOH) molten pellets. To this solution, 1 M cobalt nitrate ($Co(NO_3)_2{\cdot}6H_2O$) and 2 M manganese nitrate ($Mn(NO_3)_2{\cdot}6H_2O$) solutions were added and then mixed thoroughly by stirring the solution for a few minutes to ensure the homogeneity. The solution was then transferred into an

autoclave containing a Teflon vessel and kept in the furnace for 24 hours at a constant temperature of 180 °°C. After completion of the reaction, the autoclave containing solution was cooled down naturally. Finally, the precipitate was washed several times by using water and ethanol to remove the impurities, dried, and annealed at 500 °C for 5 hours and collected for characterization. Possible chemical reactions resulting in the formation of pure $CoMn_2O_4$ nanostructured material can be expressed by Eqs. (1) - (3):

$$Mn^{2+} + 2OH^- \rightarrow Mn(OH)_2 \quad (1)$$

$$Co^{2+} + 2OH^- \rightarrow Co(OH)_2 \quad (2)$$

$$2Mn(OH)_2 + Co(OH)_2 + 1/2O_2 \rightarrow CoMn_2O_4 + 3H_2 \quad (3)$$

Surface characterization

The crystal structure of the $CoMn_2O_4$ material was studied by powder XRD (XRD, Rigaku miniflux (II)-c). The Debye-Scherer formula was used to evaluate the average crystallite size of the synthesized material.

$$d = \frac{0.9\lambda}{\beta \cos\theta} \quad (4)$$

where λ is the x-ray wavelength, β is the full-width half-maximum, θ is the Bragg diffraction angle, and d is the crystallite size.

Fourier-transform infrared (FT-IR) study was performed using a Perkin Elmer spectrometer with KBr pellet-based samples in the frequency range between 4000 and 400 $cm^{-1.}$ Morphology of the synthesized material was viewed by field emission scanning electron microscopy (FE-SEM) and high-resolution electron microscopy (HR-TEM) using a Hitachi H7650.

Electrochemical measurements and preparation of the electrode

The electrochemical behaviour of $CoMn_2O_4$ nanostructures was characterized by cyclic voltammetry (CV), galvanostatic charge-discharge (GCD) and electrochemical impedance spectroscopy (EIS) analyses. These measurements were performed using a conventional three-electrode system with platinum wire as the counter electrode and Ag/AgCl/ sat. KCl as the reference electrode. For the preparation of working electrodes, the $CoMn_2O_4$ material was mixed with polyvinylidene difluoride and activated carbon added to the above mixture in order to achieve homogeneity. The prepared material was brush coated onto nickel foil (NF). The mass of the loaded active material ranged from 0.4 and 0.5 mg. All electrochemical experiments were conducted at room temperature. The specific capacitance value was calculated from cyclic voltammetry and Galvanostatic charging/discharging curves. Cyclic voltammetry was recorded to determine the charge-storage capacity within a potential window of 0.0 to 0.5 V (*vs.* Ag/AgCl sat. KCl) at various scan rates from 5 to 100 mV s^{-1} using CHI (7081C) electrochemical workstation (USA). For testing charging and discharging properties, chronopotentiometry measurements at various constant currents (2-4 A g^{-1}) were applied between 0.0 and 0.5 V (*vs.* Ag/AgCl sat. KCl). Electrochemical impedance spectrum was also carried out at 0.5 V *vs*. Ag/AgCl sat. KCl, in the frequency region between 1 MHz and 1 Hz.

Results and discussion

XRD analysis

The structure and phase purity of the prepared $CoMn_2O_4$ material after calcining were studied by X-ray powder diffraction, as shown in Figure 1. All reflections could be indexed as body-centred-

tetragonal (bct) phase (JCPDS no. 77-0471) with a distorted spinel structure. The sharpening of the peaks is observed, which indicates the improvement in crystalline quality. No residues or contaminants have been detected in the XRD pattern, which indicates the complete transformation from Co–Mn-DH (double hydroxide) precursors to $CoMn_2O_4$ and the high phase purity of the sample. The mean crystallite size was calculated from the (211) peak with the Scherrer formula given by Eq. (4), and the size is found to be 34 nm for the $CoMn_2O_4$ sample [15,16]

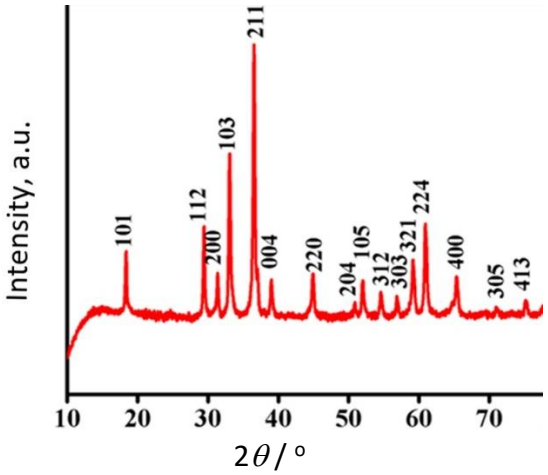

Figure 1*. XRD patterns of $CoMn_2O_4$ nanostructured material*

FT-IR analysis

FT-IR spectrum of the $CoMn_2O_4$ nanostructured material prepared by DH (double hydroxide) treatment is shown in Figure 2. The peaks observed around 3415 (broad) and 2921 (small) cm^{-1} correspond to the stretching vibration of hydrogen-bonded hydroxyl groups. The shoulder peak at 1626 cm^{-1} corresponds to the bending mode of absorbed water molecules. The characteristic absorption small bands at around 621 cm^{-1} are attributed to the vibration of the tetrahedral oxygen environment (mainly cobalt oxide), while the peak observed at 493 cm^{-1} can be correlated to the vibration of the octahedral oxygen environment (mainly manganese oxide), which further demonstrate the formation of pure $CoMn_2O_4$ by annealing at 500 °C [17].

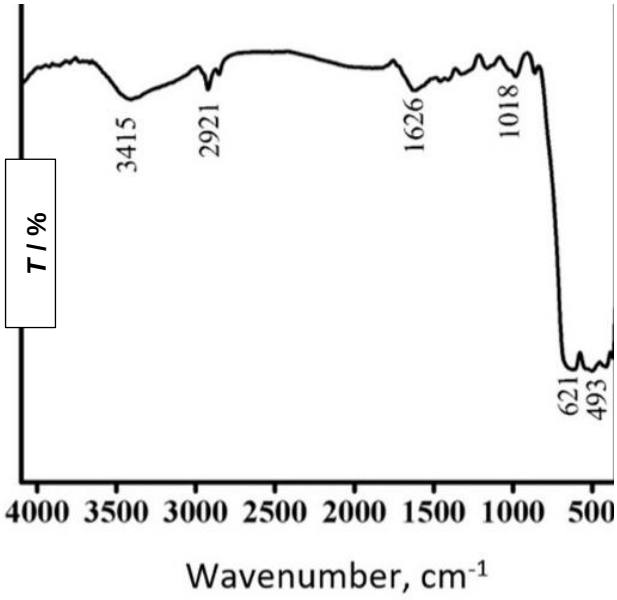

Figure 2. *FT-IR spectrum of $CoMn_2O_4$ nanostructured material*

Morphology analysis

The morphology of the prepared $CoMn_2O_4$ material was investigated by FE-SEM and HR-TEM with different magnifications. Figure 3(a) displays FE-SEM images of $CoMn_2O_4$ prepared by double hydroxide solution treatment, while the corresponding HR-TEM images are shown in Figure 3 (b and c). Clearly, the prepared $CoMn_2O_4$ is composed of disordered cubic-like nanostructure with small agglomerates and rough surfaces. In Figure 3(d), the selected area diffraction (SAED) pattern displays well-defined rings, representing the characteristic polycrystalline nature of $CoMn_2O_4$ and not amorphous. It is anticipated that this material can absorb and strongly retain electrolyte ions, ensuring sufficiently fast faradic reactions, specifically at high current densities. In addition, this kind of morphology can afford higher active sites and a specific surface area leading to high performance in the electrochemical energy storage system.

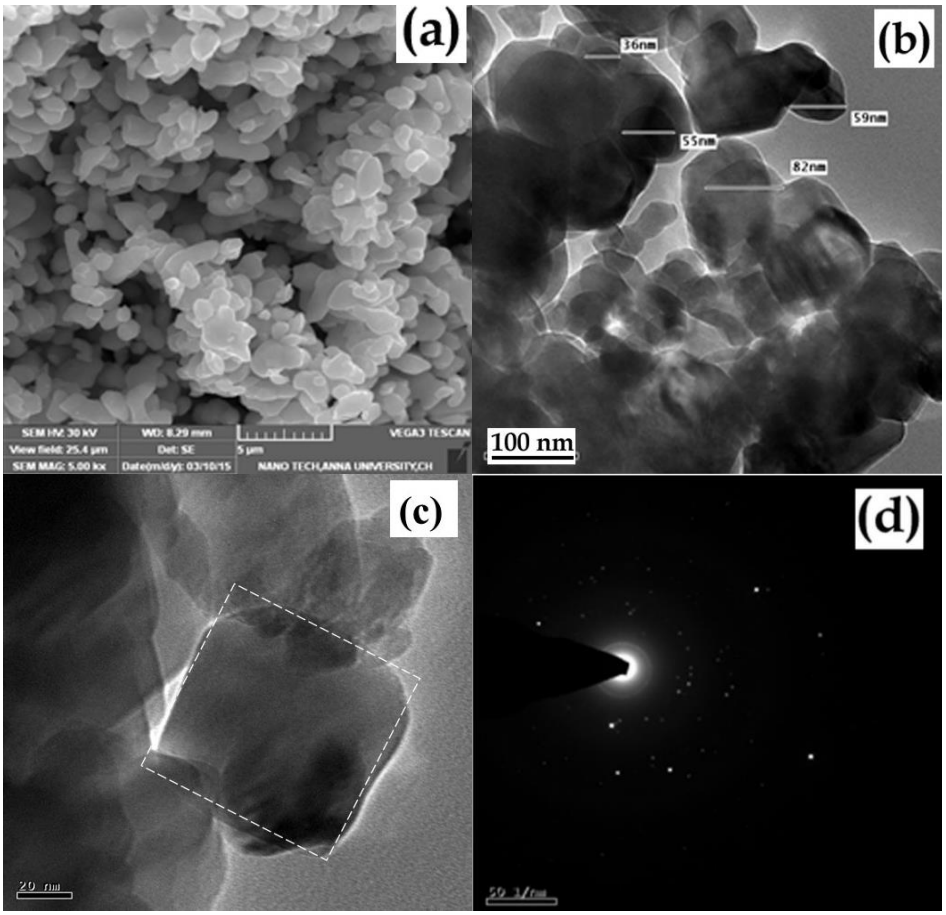

Figure 3. *(a) FE-SEM, (b, c) HR-TEM images and (d) SAED pattern of $CoMn_2O_4$ nanostructured material*

Electrochemical properties

Cyclic voltammetry analysis

Cyclic voltammetry (CV) was used to study the charge storage capacity and charge storage mechanism of the $CoMn_2O_4$ electrode. The electrochemical performance of the $CoMn_2O_4$ electrode was tested using a three-electrode working system in 2 M KOH electrolyte. The CV curves in the potential region from 0 to 0.5 V at various scan rates are shown in Figure 4(a). For the as-obtained electrode, the shape of CV curves indicates a predominant pseudocapacitive behaviour. The current values were found to increase upon increasing the scan rate due to the fast electronic and ionic transport rates between nanostructured electrode and electrolyte. At low scan rates, CV curves exhibit nearly rectangular shapes, indicating no kinetic limitations and well stability of the

supercapacitor [18]. At higher scan rates, CV curves are slightly deviated from a rectangular-like response but still demonstrate capacitive behaviour at scan rates up to 100 mVs^{-1}. This indicates the rapid current response to voltage reversal (small contact resistance) and reveals pseudocapacitive properties of the $CoMn_2O_4$ electrode.

The probable charge storage mechanism may be described ba eq. (5):

$$(CoMn_2O_4)_{surface} + K^+ + e^- = [KCoMn_2O_4]_{surface} \quad (5)$$

According to the reaction described by Eq. (5), energy storage is based on the adsorption/absorption of electroactive ions (K^+) at the surface (or near-surface) electrode region, which is undergoing charge transfer and without bulk phase transformation.

The specific capacitance values were calculated using eq. (6):

$$C_s = \frac{1}{vm\left(V_a - V_c\right)} \int_{V_a}^{V_c} IV\mathrm{d}V \quad (6)$$

where

$$\int_{V_a}^{V_c} IV\mathrm{d}V$$

is the integral value during the cathodic scan, m is the mass of the active electrode material loaded on the substrate, v is the scan rate, and $V_a - V_c$ is the working potential window range. Based on Figure 4(a) and eq. (6), specific capacitance values of $CoMn_2O_4$ electrode material were calculated to be 762.4, 601.35, 454.08, 292.39 and 256.91 F g^{-1}, for 5 , 10, 25, 50 and 100 mV s^{-1}, respectively. From the CV results, the modified electrode reveals the pseudocapacitive behaviour. The specific capacitance value of the electrode material decreased as the scan rate increased, which may be owing to the availability of cations near the surface of the electrode, which cannot be effectively utilized on the surface of the electroactive material. Anyhow, the CV testing of the electrode under scan rate of 5 mV s^{-1} and obtained C_s of 762.4 F g^{-1} suggests a potential use of such material in SCs used in high power applications [19]. Table 1 shows that here obtained specific capacitance of $CoMn_2O_4$ is higher than found in earlier reported studies and other ternary/binary transition metal oxides.

Table 1. *Comparison of the specific capacitance value of $CoMn_2O_4$ with earlier studies.*

Material	Synthesis method	Specific capacitance, F g^{-1}	Electrolyte	Reference
$NiCo_2O_4$	Solvothermal	758 at 1 A g^{-1}	2 M KOH	[20]
V_2O_5/carbon	Electrospinning	150 at 1 mA	6 M KOH	[21]
Carbon/Nickel	Electrospinning	103.8 at 0.5 A g^{-1}	6 M KOH	[22]
$CoMn_2O_4$	Hydrothermal	140.6 mAh g^{-1} at 1 mA cm^{-2}	3 M KOH	[23]
$CoMn_2O_4$	Electrospinning	121 at 5 mV s^{-1}	3 M NaOH	[24]
$CoMn_2O_4$	Hydrothermal	762.4 at 5 mV s^{-1}	2 M KOH	Present work

Charging-discharging analysis

The charge/discharge analysis confirms the excellent reversibility characteristics with a nearly symmetric charging/discharging profile. Galvanostatic charge-discharge analysis was carried out at different current densities of 1, 2, 3 and 4 A g^{-1} in the potential window range between 0 to 0.5 V, as shown in Figure 4(b). At high current densities, the discharge curves are nearly symmetrical to the corresponding charge curves, which indicates a highly capacitive nature of the $CoMn_2O_4$ electrode and electrochemical reversibility of the underlying faradaic reaction. The nearly symmetrical charge/discharge profiles are in good agreement with almost rectangular CV curves.

The apparent deviation from straight lines in the charge-discharge plots is obtained at low currents, indicating some inhibition of the faradic pseudocapacitive reaction of as-synthesized material [25]. Also, the curves are highly symmetric at peak values, showing that the electrode has low internal resistance. Furthermore, the specific capacitance values were calculated using Eq. (7),

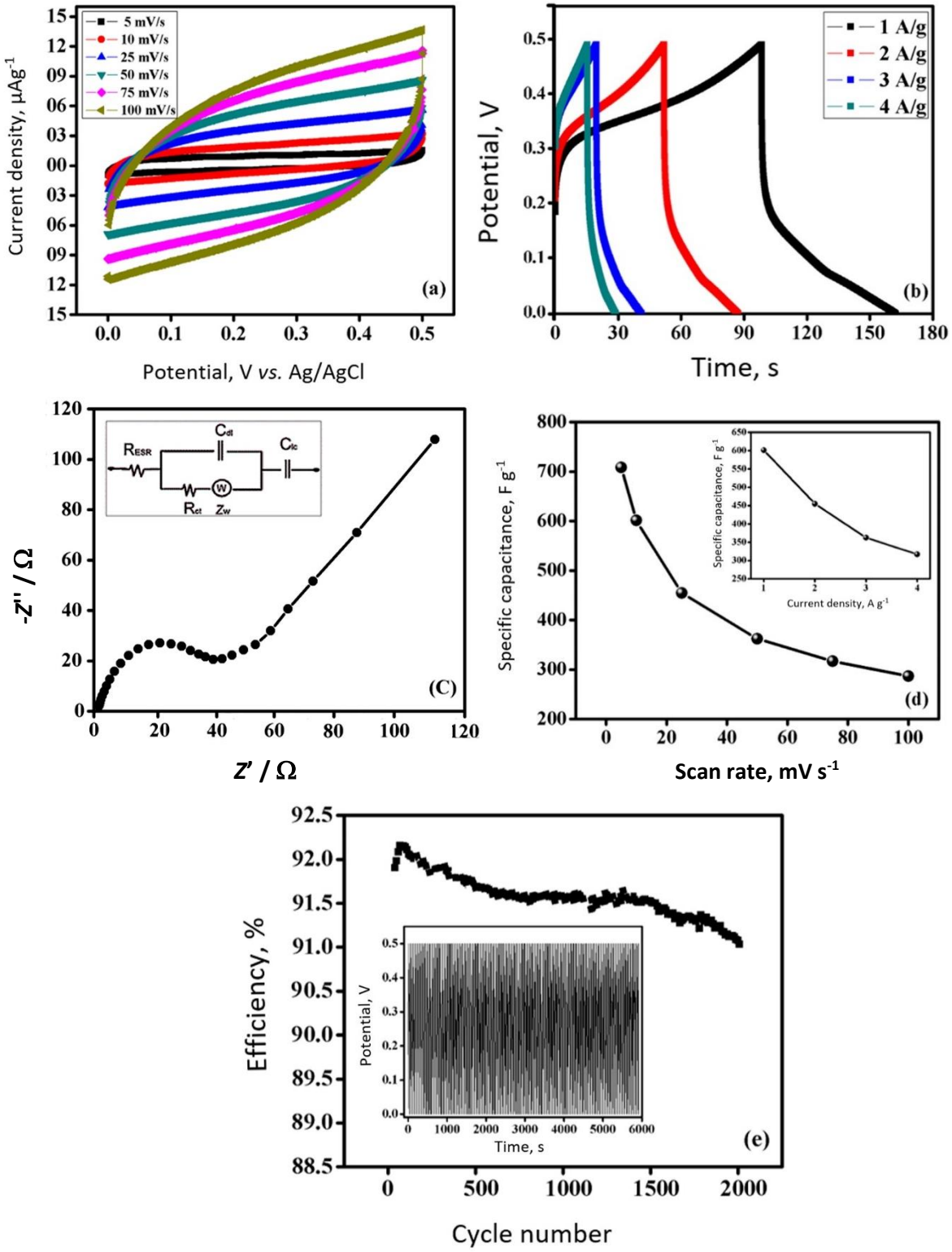

Figure 4. *(a) CV curves of $CoMn_2O_4$ nanostructured material in 2 M KOH at different scan rates; (b) GCD curves at different current densities; (c) Nyquist plot at 0.5V; (d) variation of specific capacitance with scan rate; insert: variation of specific capacitance with current density applied; (e) coulombic efficiency during 2000 charge-discharge cycles recorded at a current density of 2 A g^{-1}; insert: few long term cycles*

$$C_s = \frac{It_d}{m\nabla V} \quad (7)$$

where, I is the constant current applied, t_d is discharge time, m is the mass of the electroactive material loaded, and ∇V is the potential difference (0.5 V) [24]. Specific capacitance values calculated from charging/discharging curves in Figure 4(b) and eq. (7) are presented in the inset of Figure 4(d). The specific capacitance values of the $CoMn_2O_4$ material calculated from GCD results concord with CV results.

Long-term cycle charge/discharge analysis was also carried out to evaluate the cyclic stability of the prepared $CoMn_2O_4$ electrode material. A constant current density of 2 A g^{-1} was applied to examine the $CoMn_2O_4$ electrode in 2 M KOH electrolyte, and 2000 charging-discharging cycles were performed. The results are in the form of coulombic efficiency *vs.* cycle number presented in Figure 4(e). The coulombic efficiency of the $CoMn_2O_4$ electrode was calculated using the relation,

$$\eta = (t_d / t_c)\ 100 \quad (8)$$

where, η is coulombic efficiency, t_d is the discharge time and t_c is charging time derived from charge-discharge curves. Figure 4(e) shows a gradual increase of the coulombic efficiency during the first few cycles, which indicates a certain electro-activation process of the electrode under given testing conditions (voltage range of 0 to 0.5 V and current density of 2 A g^{-1}). After that, the coulombic efficiency slightly decreased with the cycling but retained 91.2 % of the initial efficiency after 2000 cycles.

Electrochemical impedance spectroscopy analysis

The electrochemical impedance spectroscopy analysis is exploited to evaluate the electrochemical properties of $CoMn_2O_4$ material. Figure 4(c) shows the Nyquist plot of the $CoMn_2O_4$ electrode in 2 M KOH, measured 0.5 V within the frequency region of 1 MHz to 1 Hz. The plot reveals a distinct semicircle at high frequencies and a sloping straight line in the lower frequency region. The semicircle impedance response in the high-frequency region corresponds to the charge-transfer resistance at the electrode/electrolyte interface, and the straight line observed at low frequencies corresponds to the diffusion process of electroactive species (Warburg impedance) [26]. The equivalent circuit diagram proposed to fit the impedance spectrum is shown in the inset of Figure 4(c). The resistance (R_s), which involves ohmic resistance of the active material and electrolyte, as well as the contact resistance at the interface between the active material and current collector, is obtained as the high-frequency intercept of the semicircle at the real impedance axis. Faradaic interfacial charge-transfer resistance (R_{ct}) is associated with the diameter of the semicircle in the high-frequency range. The Warburg impedance, which indicates the frequency dependence of ion diffusion [27], is probably related to the diffusion of K^+ within the surface and near-surface layer according to the charge storage mechanism described by eq. (5).

Conclusion

In summary, spinel $CoMn_2O_4$ nanostructure was successfully synthesized using facile hydrothermal route at 180 °C followed by annealing at 500 °C. The prepared material was characterized by XRD, FT-IR, FE-SEM and HR-TEM analyses, revealing a nanostructured material of polycrystalline nature. The electrochemical properties were investigated in 2 M KOH aqueous electrolyte using cyclic voltammetry, charge-discharge, long-term cycle stability performance and electrochemical impedance spectroscopy measurements. The maximum specific capacitance of 762.4 F g^{-1} was obtained from CV measurements at 5 mV s^{-1}, while about 600 F g^{-1} was obtained by galvanostatic charging-discharging at 1 A g^{-1}. The material showed sufficient cycling stability over

2000 cycles. The results demonstrate that the spinel-$CoMn_2O_4$ nanostructure should be a promising electrode material for supercapacitor applications.

References

[1] L. Li. H. Hu, S. Ding, *Inorganic Chemistry Frontiers* **5(7)** (2018) 1714-1720. https://doi.org/10.1039/C8QI00121A

[2] C. Zhu, R.-G. Lu, L. Tian, Q. Wang, *IEEE Vehicle Power and Propulsion Conference* (2006) 24172345. https://doi.org/10.1109/VPPC.2006.364372

[3] Y. Wang, Y. Song, Y. Xia, *Chemical Society Reviews* **45(21)** (2016) 5925-5950. https://doi.org/10.1039/C5CS00580A

[4] X. Lu. D. Zheng. T. Zhai. Z. Liu. Y. Huang. S. Xie. Y. Tong, *Energy and Environmental Science* **4** (2011) 2915-2921. https://doi.org/10.1039/C1EE01338F

[5] V. Venkatachalam. R. Jayavel, *International Journal of ChemTech Research* **6(13)** (2014) 5404-5407. https://sphinxsai.com/2014/ch_vol6_no13/5/(5404-5407)%20014.pdf

[6] B. Wang. J. S. Chen. Z. Wang. S. Madhavi. X. W. Lou, *Advanced Energy Materials* **2 (10)** (2012) 1188-1192. https://doi.org/10.1002/aenm.201200008

[7] D. H. Deng. H. Pang. J.M. Du. J. W. Deng. S. J. Li. J. Chen. J. S. Zhang, *Crystal Research Technology* **47(10)** (2012) 1032-1038. https://doi.org/10.1002/crat.201200161

[8] S. L. Kuo. N. L. Wu, *Electrochemical and Solid-State Letters* **8** (2005) A495-A499. https://doi.org/10.1149/1.2008847

[9] V. Venkatachalam. A. Alsalme. A. Alghamdi. R. Jayavel, *Journal of Electroanalytical Chemistry* **756(1)** (2015) 94-100. https://doi.org/10.1016/j.jelechem.2015.08.019

[10] V. Venkatachalam, R. Jayavel, *AIP Conference Proceedings* **1665** (2015) 140016. https://doi.org/10.1063/1.4918225

[11] Y. Zhang, Y. Ru, H.-L. Gao, S.-W. Wang, J. Yan, K.-Z. Gao, X.-D. Jia, H.-W. Luo, H. Fang, A.-Q. Zhang, L.-Z. Wang, *Journal of Electrochemical Science and Engineering* **9** (2019) 243-253. https://doi.org/10.5599/jese.690

[12] Y. Xu, X.F. Wang. C. An, Y. Wang. L. Jiao, H. Yuan, *Journal of Materials Chemistry A* **2** (2014) 16480-16485. https://doi.org/10.1039/C4TA03123G

[13] S. Jiang, T. Shi, H. Long, Y. Sun, W. Zhou, Z. Tang, *Nanoscale Research Letters* **9** (2014) 492-500. https://doi.org/10.1186/1556-276X-9-492

[14] L. Ren, J. Chen, X. Q. Wang, M. J. Zhi, J. W. Wu, X. H. Zhang, *RSC Advances* **5** (2015) 30963-30969. https://doi.org/10.1039/C5RA02663F

[15] X. Shi, F. Zheng, N. Yan, Q. Chen, *Dalton Transactions* **43** (2014) 13865-13873. https://doi.org/10.1039/C4DT01686F

[16] H. T. Zhang, X. H. Chen, *Nanotechnology* **17(5)** (2006) 1384-1390. https://doi.org/10.1088/0957-4484/17/5/037

[17] S. A. Hosseini, D. Salari, A Niaei, F. Deganello, G. Pantaleo, P. Hojati, *Journal of Environmental Science Health A* **46(3)** (2011) 291-296. https://doi.org/10.1080/10934529.2011.539093

[18] K. S. Ujjain, P. Ahuja, R. K. Sharma, *Journal of Materials Chemistry A* **3** (2015) 9925-9931. https://doi.org/10.1039/C5TA00653H

[19] S. G. Mohamed, C. J. Chen, C. K. Chen, S. F. Hu, R. S. Liu, *ACS Applied Materials Interfaces* **6 (24)** (2014) 22701-22708. https://doi.org/10.1021/am5068244

[20] E. Jokar, A. I. Zad, S. Shahrokhian, *Journal of Solid-State Electrochemistry* **19** (2015) 269-276. https://doi.org/10.1007/s10008-014-2592-y

[21] B. H. Kim, C. H. Kim, K. S. Yang, A. Rahy, D. J. Yang, *Electrochimica Acta* **83 (30)** (2012) 335-340. https://doi.org/10.1016/j.electacta.2012.07.093

[22] D. Gao, L. Wang. X. Xia. H. Qiao. Y. Cai. F. Huang. K. Gupta. Q. Wei. S. Kumar. *Journal of Engineered Fibers and Fabrics* **8 (4)** (2013) 108-113. https://doi.org/10.1177%2F155892501300800405

[23] F. Chen, Z. Wang, S. Huo, S. Ji, H. Wang, P. Zhou. *Materials Letters* **237 (15)** (2019) 209-212. https://doi.org/10.1016/j.matlet.2018.11.100

[24] S. Alkhalaf, C. K. Ranaweera, P. K. Kahol, K. Siam, H. Adhikari, S. R. Mishra, F. Perez, B. K. Gupta, K. Ramasamy, R .K Gupta, *Journal of Alloys and Compounds* **692 (25)** (2017) 59-66. https://doi.org/10.1016/j.jallcom.2016.09.005

[25] T. Anitha, A. E. Reddy, R. Vinodh, H. J. Kim, Y. R. Cho, *Journal of Energy Storage* **30** (2020) 101483. https://doi.org/10.1016/j.est.2020.101483

[26] J. L. Liu, L. Zhenfan, X. Qu, *Electrochimica Acta* **66(1)** (2012) 302-305. https://doi.org/10.1016/j.electacta.2012.01.095

[27] T. Antony Sandosh, A. Simi, *Chemical Papers* **75** (2021) 2295-2304. https://doi.org/10.1007/s11696-020-01448-z